AUTOMATIC MRI BRAIN TISSUE SEGMENTATION USING A HYBRID STATISTICAL AND GEOMETRIC MODEL

Albert Huang[1], Rafeef Abugharbieh[1], Roger Tam[2] and Anthony Traboulsee[2]

[1]Dept. of Elec. & Comp. Eng., The University of British Columbia, Vancouver, BC, V6T 1Z4, Canada
[2]Dept. of Medicine, The University of British Columbia, Vancouver, BC, V6T 1Z3, Canada

ABSTRACT

This paper presents a novel hybrid segmentation technique incorporating a statistical as well as a geometric model in a unified segmentation scheme for brain tissue segmentation of magnetic resonance imaging (MRI) scans. We combine both voxel probability and image gradient and curvature information for segmenting gray matter (GM) and white matter (WM) tissues. Both qualitative and quantitative results on synthetic and real brain MRI scans indicate superior and consistent performance when compared with standard techniques such as SPM and FAST.

1. INTRODUCTION

Magnetic resonance imaging (MRI) provides an excellent non-invasive method for neurologists to examine the brain of patients with neurodegenerative diseases such as Multiple Sclerosis (MS). The ability to diagnose these diseases systematically and quantitatively with MRI brings exciting developments not only to the study of the pathology, but also to the clinical trials of drug treatments [1].

An important biomarker for patients with neurodegenerative disease is tissue atrophy due to neural-axonal loss in the brain and spinal cord [2]. A typical rate of brain atrophy observed for patients with MS is 0.6% to 0.8% annually, which is 2-3 times the normal rate [3] and is thus a good indicator of disease progression. As a result, one application of automatic brain tissue segmentation methods is to provide systematic and quantitative analysis of brain volumes.

Manual segmentation of 3D volumetric data is difficult and time-consuming, and is prone to intra- and inter-rater errors. Fully and semi- automatic methods have been developed to provide accurate, robust, and reproducible alternatives. Van Leemput *et al*. [4] applied a statistical maximum likelihood (ML) approach for bias field correction and tissue classification of brain MRI. Tissues are modeled as a mixture of independent Gaussian or polynomial distributions with parameters estimated using the expectation-maximization (EM) algorithm. Markov random fields (MRF) were introduced to determine the most probable tissue type. Similar statistical techniques have been used in analysis tools such as the FMRIB (functional MRI of brain) Automatic Segmentation Tool (FAST) [5]. Statistical Parametric Mapping (SPM) [6], on the other hand, utilizes a brain template and performs voxel-based morphometry. In our investigations, we observed, as described in Section 4, a lack of consistency in performance when using these standard techniques with synthetic and real MRI scans.

Other segmentation approaches based on geometric information such as deformable models have been used. Those depend heavily on the accuracy of initializations and are prone to leakage at noisy and weak edges frequently observed in medical images. To solve this problem, researchers have tried to combine statistical and geometric information for aiding the model convergence. Leventon *et al*. [7] and Chen *et al*. [8] introduced a shape model prior into the active contour formulation and Ho *et al*. [9] introduced a modulating statistical force to the model for stabilizing the solution.

Our proposed method combines the statistical and geometric information and aims to provide a fully automated 3D segmentation flow. However, without knowing any shape prior or directly changing the overall energy equation like other proposed methods, we improve the geodesic active contour method by incorporating voxel-wise probability with image gradient and curvature information in the feature image, based on which the active contour is then evolved in 3D.

2. METHOD

Before processing an MRI scan, the brain volume is extracted by removing the exterior skull and the background. We utilize the Brain Extraction Tool (BET) which applies a deformable surface model for automatic brain and non-brain segmentation from an estimated center of gravity [10]. We are also developing our own brain extraction algorithm to overcome problems observed with the BET method. A noise reduction filter is then introduced

to improve the image signal-to-noise ratio (SNR). Since edge information is essential for active contour propagation, an edge-preserving anisotropic diffusion filter [11] is applied.

2.1 Modeling voxel statistics

To determine the probability of each voxel belonging to a certain tissue type, we study the image intensity histogram. Each tissue type is modeled by a Gaussian distribution with the mean determined by the peak position and the variance determined by the width. The probability density function, $p(x)$, of this mixture model can be described as:

$$p(x) = \sum_{i=0}^{K-1} \alpha_i p_i(x \mid \Phi_i) \qquad (1)$$

where x is the voxel intensity, i is the class index, K is the number of classes, α_i is the class proportion, and $p_i(x|\Phi_i)$ is the probability of the voxel belonging to the i-th class with the distribution parameter set Φ_i. The class probability density functions are Gaussians in our case, and we need to determine the parameters that describe these distributions.

Based on the mean intensity estimates derived from tree-structured K-means algorithm for gray matter (GM), white matter (WM), and cerebrospinal fluid (CSF), three Gaussian models are fitted to the intensity histogram using the EM algorithm. The E or expectation step (2) of this algorithm calculates the expected membership of each voxel to each class. The M or maximization step (3) then finds the next parameter sets that maximize the likelihood with the expected membership values and the current parameter set.

$$Q(\Phi_i \left| \Phi_i^m \right.) = E_i[\log p_i(x, i \left| \Phi_i \right.) \left| x, \Phi_i^m \right.] \qquad (2)$$

$$\Phi_i^{m+1} = \arg\max_{\Phi_i} Q(\Phi_i \left| \Phi_i^m \right.) \qquad (3)$$

where Φ_i is the parameter set for the i-th component class, and m is the iteration number. The EM algorithm iteratively updates the model parameters accordingly. Once we obtain the parameter sets, probability maps showing the probability that each voxel belongs to each class, can be generated.

2.2 Geodesic active contour

A geodesic active contour [12] framework transforms the traditional energy minimization problem of a deformable model into finding the geodesic or the minimal distance curve distance in a Riemannian space. A gradient descent search is performed for finding the minima. With steepest gradient descent and the Euler-Lagrange equation, the initial curve C_0 is deformed according to the evolution equation:

$$\frac{\partial C}{\partial t} = g(I)\kappa\vec{N} - (\nabla g \cdot \vec{N})\vec{N} \qquad (4)$$

where κ is the Euclidean curvature, $\vec{N}$ is the inner unit normal, g is a general function of intensity I. The flow $\partial C/\partial t = \kappa\vec{N}$ is the Euclidean heat flow equation satisfying the geometric smoothing property. To represent (4) using a level-set approach, we embed (4) in a level-set of a function u, and search for the steady state solution of (5).

$$\frac{\partial u}{\partial t} = g\left|\nabla u\right|\kappa + \nabla g \cdot \nabla u \qquad (5)$$

A constant velocity term c is introduced in (6) as a balloon force to increase the attraction of the deforming contour to the boundary, and the final level-set surface moves according to (7).

$$\frac{\partial C}{\partial t} = g(I)(c+\kappa)\vec{N} - (\nabla g \cdot \vec{N})\vec{N} \qquad (6)$$

$$\frac{\partial u}{\partial t} = g\left|\nabla u\right|(c+\kappa) + \nabla g \cdot \nabla u \qquad (7)$$

2.3 Initial contour

The level-set approach requires an initial contour as the zero level-set from which the active contour will then propagate. To choose a suitable contour for each region to be segmented, we take the probability map for each class and apply a low threshold of 0.1 on the probability so that only voxels with sufficient probability remain. Then morphological thinning and pruning are performed, and the resulting skeleton is used as the initial contour.

2.4 Probability-weighted stopping function

The general function g is used as the speed and halting feature for the evolving curve, and is generally chosen as in (8) where ρ=1 or 2, and $\hat{I}$ is a smoothed version of I. An ideal edge has a feature value g of zero.

$$g(I) = \frac{1}{1 + \left|\nabla \hat{I}\right|^{\rho}} \qquad (8)$$

However, with real images, the feature image is never truly zero at boundaries. Thus, the propagating curve never stops at the boundaries, only to evolve very slowly. We propose a modified feature function which is weighted based on the voxel probability. The signed weighting function would determine the propagation or shrinking of the contour for stable convergence of the solution.

The propagation and shrinking varies in speed depending on the voxel probability. If the voxel has a high probability of belonging to a part of the contour, we expect a fast propagation. If the voxel has a low or zero probability of belonging to a part of the contour, we expect a fast shrinkage. If the voxel lies in between, we expect a slow variation of propagation or shrinking (Fig. 1). Tissue probability of 0.5 is used as a switching point for the evolution direction because when the posterior probability of a voxel exceeds 50%, the tissue/non-tissue competition and classification can thus be determined.

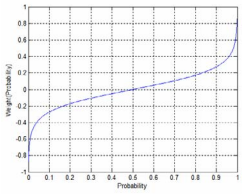

Fig. 1. Proposed probability weighting function

The proposed weighting function is derived from the sigmoid function (9). By taking the inverse and substituting $y=f_i(x)$ and $x=w_i(f_i(x))$, we obtain the weighting function in (10) for the i-th class at position x given the voxel-wise probability $f_i(x)$. The higher the class probability is, the higher the weighting value is, and the faster the contour convergence is.

$$y = 1/(1+e^{-x}) \qquad (9)$$

$$w_i(f_i) = \mathrm{sgn}(f_i(x)-0.5)\cdot \max\left(1, \left|-\frac{\ln(1/f_i(x)-1)}{\varphi}\right|\right) \qquad (10)$$

where φ is a slope scaling factor. The contour would thus be constrained from propagating further outside the less probable region. The new feature function is therefore (11) instead of (8). Each tissue class type has a different feature map since each tissue class has a different probability map.

$$\hat{g}_i(I) = g(I)\cdot w_i(f_i) \qquad (11)$$

The geodesic active contour evolves under the same conditions as described above except that each contour now has its own feature map based on the proposed feature function (Fig. 2).

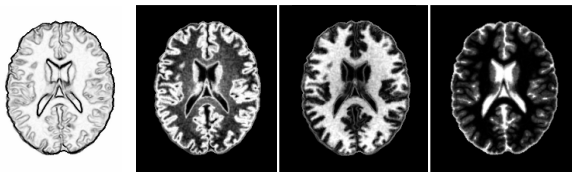

Fig. 2. General sigmoid feature map and our modified feature maps for GM, WM, and CSF (left to right).

3. DATA

Our tests utilized 18 synthetic volumes obtained from the BrainWeb simulated brain database [13-16] of the McConnell Brain Imaging Centre. The T1-weighted modality data and the provided phantom are 1mm×1mm×1mm in spacing. Noise level varies at 0%, 1%, 3%, 5%, 7% and 9%, and intensity non-uniformity varies at 0%, 20% and 40%.

The 20 normal MR brain data sets and their manual segmentations were provided by the Center for Morphometric Analysis at Massachusetts General Hospital and are available at http://www.cma.mgh.harvard.edu/ibsr/. We selected only 10 datasets out of these 20 T1-weighted spoiled gradient echo volumes from the International Brain Segmentation Repository (IBSR) because of the existing intensity inhomogeneity problem which is not the focus of this study. The data are acquired coronally with 1mm×3.1mm×1mm in spacing.

4. RESULTS AND DISCUSSIONS

We evaluated our results both quantitatively and qualitatively with the synthetic BrainWeb and real IBSR MRI data.

4.1. Quantitative results

Our results indicate that when comparing the 18 synthetic BrainWeb volumes with the provided phantom, our proposed method outperforms both SPM and FAST on average (Table I). SPM and FAST sacrifices WM for GM sensitivity performance, whereas our proposed method takes a more balance approach.

TABLE I
AVERAGE PERFORMANCE OF 18 BRAINWEB VOLUMES

Method	Metric	Gray Matter (%)		White Matter (%)	
		Mean	*Std Dev*	*Mean*	*Std Dev*
SPM2	*Similarity Index*	*89.45*	*3.79*	*86.69*	*9.04*
	Misclassification	*5.17*	*2.25*	*3.72*	*2.07*
	Vol. Difference	*18.98*	*11.93*	*21.44*	*13.26*
	Sensitivity	*97.73*	*1.23*	*77.96*	*12.92*
	Specificity	*94.00*	*3.16*	*99.88*	*0.12*
FAST	*Similarity Index*	*88.04*	*2.01*	*88.42*	*5.09*
	Misclassification	*5.48*	*1.14*	*3.40*	*1.20*
	Vol. Difference	*7.64*	*6.65*	*17.95*	*8.70*
	Sensitivity	*91.31*	*1.28*	*80.68*	*7.90*
	Specificity	*95.42*	*1.66*	*99.73*	*0.27*
Proposed Method	*Similarity Index*	*91.40*	*2.56*	*94.45*	*2.16*
	Misclassification	*3.66*	*0.99*	*1.83*	*0.76*
	Vol. Difference	*5.03*	*4.47*	*5.06*	*1.65*
	Sensitivity	*89.16*	*4.49*	*93.64*	*0.42*
	Specificity	*98.36*	*0.10*	*99.07*	*0.97*

When comparing 10 real IBSR volumes with expert segmentation masks (Table II), our results are comparable with SPM and outperform FAST. We also achieved better consistencies with lower overall standard deviations.

TABLE II
AVERAGE PERFORMANCE OF 10 IBSR VOLUMES

Method	Metric	Gray Matter (%)		White Matter (%)	
		Mean	*Std Dev*	*Mean*	*Std Dev*
SPM2	*Similarity Index*	*83.08*	*1.96*	*83.30*	*1.61*
	Sensitivity	*81.14*	*2.61*	*77.22*	*2.82*
	Specificity	*77.12*	*2.56*	*95.40*	*1.07*
FAST	*Similarity Index*	*73.81*	*13.06*	*74.73*	*6.33*
	Sensitivity	*68.94*	*17.15*	*86.59*	*7.09*
	Specificity	*77.46*	*4.25*	*73.12*	*17.99*
Proposed Method	*Similarity Index*	*80.03*	*3.11*	*83.69*	*2.36*
	Sensitivity	*73.74*	*7.77*	*85.13*	*2.86*
	Specificity	*90.42*	*2.30*	*89.65*	*2.60*

4.2. Qualitative results

We show a single slice result from our synthetic BrainWeb (Fig. 3) and real IBSR (Fig. 4) volumes, and highlight some problematic regions apparent when using the other methods. With BrainWeb data, our method preserved small holes and details unlike SPM2 and FAST. With IBSR data, SPM2 masks and our masks are comparable with the manual segmentation, whereas FAST produced masks too smooth.

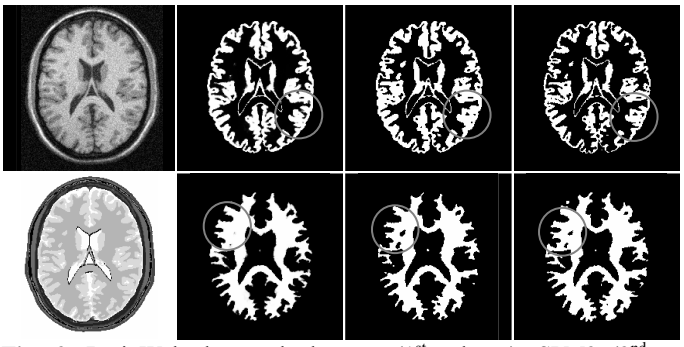

Fig. 3. BrainWeb data and phantom (1st column), SPM2 (2nd column), FAST (3rd column), and our results (4th column).

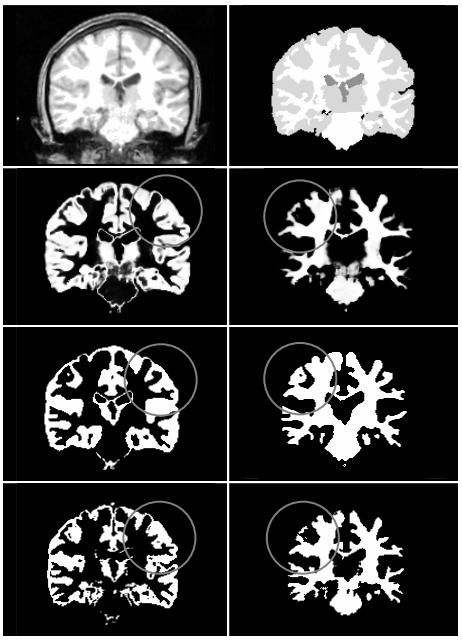

Fig. 4. IBSR data and manual segmentation mask, SPM2, FAST, and our results (top to bottom).

5. CONCLUSION

This paper introduced a modified geodesic active contour by combining statistical and geometric information into the feature image to aid with GM and WM segmentation of MRI brain scans. Quantitative results for synthetic BrainWeb and real IBSR data indicated a superior, balanced, and consistent performance for our method against SPM and FAST. Qualitative results for synthetic BrainWeb and real IBSR data also showed successful and superior tissue segmentation.

6. REFERENCES

[1] D.W. Paty, D. Li, and G.J. Zhao, *MRI in multiple sclerosis – Implications for diagnosis and treatment (2nd Edition)* [print], 1999.

[2] D.H. Miller, "Biomarkers and Surrogate Outcomes in Neurodegenerative Disease: Lessons from Multiple Sclerosis," *NeuroRx*, vol. 1, pp. 284-294, 2004.

[3] A. Traboulsee, G. Zhao, and D.K.B. Li, "Neuroimaging in Multiple Sclerosis," *Neurologic Clinics*, vol. 23, pp. 131-148, 2005.

[4] K. Van Leemput *et al.*, "A unifying framework for partial volume segmentation of brain MR images," *IEEE Transactions on Medical Imaging*, vol. 22, no. 1, pp. 105-119, January 2003.

[5] S.M. Smith *et al.*, "Advances in functional and structural MR image analysis and implementation as FSL," *NeuroImage*, vol. 23(S1), pp. 208-219, 2004.

[6] K.J. Friston *et al.*, "Classical and Bayesian Inference in Neuroimaging: Theory," *NeuroImage*, vol. 16, pp. 465-483, 2002.

[7] M. Leventon, E. Grimson, and O. Faugeras, "Statistical shape influence in geodesic active contour," *CVPR*, 2000.

[8] Y. Chen *et al.*, "Using prior shapes in geometric active contours in a variational framework," *International Journal of Computer Vision (IJCV)*, vol. 50, no. 3, pp. 315–328, 2002.

[9] S Ho, E Bullitt, and G Gerig, "Level-Set Evolution with Region Competition: Automatic 3-D Segmentation of Brain Tumors," *International Conference on Pattern Recognition (ICPR)*, pp. 532-535, August 2002.

[10] S.M. Smith, "Fast robust automated brain extraction," *Human Brain Mapping*, vol. 17, no. 3, pp. 143-155, November 2002.

[11] P. Perona and J. Malik, "Scale-space and edge detection using anisotropic diffusion," *IEEE Transactions on Pattern Analysis Machine Intelligence*, vol. 12, pp. 629–639, 1990.

[12] V. Caselles, R. Kimmel, and G. Sapiro, "Geodesic active contours," *International Journal of Computer Vision (IJCV)*, vol. 22, no. 1, pp. 61–79, 1997.

[13] C.A. Cocosco *et al.*, "BrainWeb: Online Interface to a 3D MRI Simulated Brain Database," *NeuroImage*, vol. 5, no. 4, part 2/4, S425, 1997 -- Proceedings of 3rd International Conference on Functional Mapping of the Human Brain, Copenhagen, May 1997.

[14] R.K.-S. Kwan *et al.*, "MRI simulation-based evaluation of image-processing and classification methods," *IEEE Transactions on Medical Imaging*, vol. 18, no. 11, pp. 1085-97, November 1999.

[15] R.K.-S. Kwan, A.C. Evans, and G.B. Pike, "An Extensible MRI Simulator for Post-Processing Evaluation," *Visualization in Biomedical Computing (VBC'96)*, Lecture Notes in Computer Science, vol. 1131, pp. 135-140, Springer-Verlag, 1996.

[16] D.L. Collins *et al.*, "Design and Construction of a Realistic Digital Brain Phantom," *IEEE Transactions on Medical Imaging*, vol. 17, no. 3, pp. 463--468, June 1998.